Gas/Liquid/Liquid Three-Phase Flow Patterns and Bubble/Droplet Size Laws in a Double T-Junction Microchannel

Kai Wang, Kang Qin, Yangcheng Lu, Guangsheng Luo, and Tao Wang
The State Key Laboratory of Chemical Engineering, Dept. of Chemical Engineering, Tsinghua University, Beijing 100084, China

DOI 10.1002/aic.14758
Published online February 17, 2015 in Wiley Online Library (wileyonlinelibrary.com)

The double T-junction microchannel is a classical microstructured chemical device used to generate gas/liquid/liquid three-phase microflows. An experimental study that focused on the three-phase flow phenomena and bubble/droplet generation rules in a double T-junction microchannel was introduced. Based on the published knowledge of gas/liquid and liquid/liquid two-phase microflows, new flow patterns were carefully defined: bubble cutting flow, spontaneous break-up and bubble cutting coupling flow, and bubble/droplet alternate break-up flow. According to the classical correlations of bubble and droplet volumes and their generation frequency ratio, the operating criteria for creating different three-phase flow patterns were established and a model for the dimensionless average bubble and droplet volumes in the three-phase microflows was developed. These various three-phase microflows have great application potential in material science and flow chemistry synthesis. © 2015 American Institute of Chemical Engineers *AIChE J*, 61: 1722–1734, 2015

Keywords: double T-junction microchannel, gas/liquid/liquid flow, flow pattern, size law

Introduction

The three-phase microflows are effective platforms for the studies in various fields, including biology, chemistry, materials, and engineering.[1,2] Early in 2005, a protein crystallization process in a glass capillary was successfully demonstrated by Zheng and Ismagilov,[3] where the gas/liquid/liquid three-phase flow in microchannel was first reported and inert gas slugs were used to prevent droplet coalescence. In chemistry and chemical engineering applications, microscaled gas/liquid/liquid flow systems have been used in numerous novel reactions and separation processes, such as the controllable preparation of quantum dots,[4] the selective hydrogenation of unsaturated aldehydes in an aqueous solution,[5] enhancement of vanillin extraction in water,[6] and oxidation–extraction coupling process used in the preparation of hydrogen peroxide[7] for its controllable multiphase flow, effective mass-transfer enhancement and narrow residence time distribution in microchannels. A stable gas/liquid/liquid microflow is also a template for the preparation of novel materials, such as porous or core-shell particles.[8,9]

Compared with the relatively sufficiently studied gas/liquid and liquid/liquid two-phase microflow processes,[10,11] the generation mechanism for the gas/liquid/liquid three-phase microflow is less familiar to the researchers in this area. According to the limited literatures, the generation of a gas/liquid/liquid three-phase microflow can be achieved using a single dispersion unit, such as a cross-junction microchannel[12,13] or organized dispersion units, such as a continuous double T-junction microchannel.[14] The advantage of using a single dispersion unit is the simple device,[15] whereas the advantage of using combined dispersion units is the greater freedom provided in process control.[16] In a previous study, parallel flow-focusing microchannels were used by Hashimoto et al. to generate bubbles and droplets, respectively,[17] which were then mixed to form gas/liquid/liquid three-phase microflow. As there was no interaction between two dispersed phases in their break-up processes, this type of microchannel device has a simple control rule, and it is more appropriate for the preparation of complicated foam flows with independent bubbles and droplets. In another example of using organized dispersion units, a multistage coflowing capillary was developed for the generation of gas/liquid/liquid three-phase double emulsion.[18] This type of device has two or more continuous dispersion units, and the inner flow is mainly controlled by the phase ratio of three-phase fluids. The double T-junction is another classical three-phase microstructured chemical device, and it has great application potential in flow chemistry, especially in applications that require multistage reactant feeding, such as the selective hydrogenation process studied by Onal et al.[5] and the extraction enhancement work reported by Assmann and von Rohr.[6] In most studies that utilize a double T-junction microchannel, the gas phase is often dispersed first,[4,16] considering its compressibility and higher tension on the gas/liquid interface, which assists in the formation of a stable three-phase flow based on experimental experience. The early dispersion of gas phase is also advantageous because the flowing

Correspondence concerning this article should be addressed to K. Wang at kaiwang@tsinghua.edu.cn; G. Luo at gsluo@tsinghua.edu.cn.

bubbles are powerful break-up tools in a confined microchannel, which can be used as an intensification medium in the following droplet generation process.[14,19] In addition, with a reasonable design for the channel wetting property, not only the common gas/liquid/liquid flow with separate bubbles and droplets, but also gas/liquid/liquid double emulsion[8] can be prepared in the double T-junction microchannel, showing the versatility of this type of microchannel device.

The generation rules for bubbles and droplets are very important research issues for the controllable application of gas/liquid/liquid three-phase microflows, especially for further evaluate the mass-transfer and reaction performances in microchannels. Based on our literature review, few studies have been conducted on complicated three-phase flow patterns, and quantified equations for bubble/droplet volumes are relatively absent in the research of microfluidics. In our previous studies, a capillary-embedded double T-junction microchannel was tested to generate gas/liquid/liquid three-phase microflows. The main contribution of that paper was the discovery of a periodic bubble cutting effect in the continuous phase.[14] As an in-depth research, this article introduces a systematic experimental study on the generation processes of bubbles and droplets in an ordinary double T-junction microchannel. The complicated three-phase flow phenomena are exhibited and systematic operating criteria to control these flow patterns are provided. A model to calculate the average bubble and droplet volumes is developed, based on the periodic flow pattern and the published size laws of bubbles and droplets in common gas/liquid and liquid/liquid two-phase microflows.

Experimental

Experimental setup and equipment

The experiment was conducted using the platform shown in Figure 1a. In the feeding system for the three-phase fluids, all the flow rates, which ranged from 30 to 800 μL/min, were controlled by syringe pumps (LSP02-1B, Longer) with gas tight syringes (1 or 5 mL, Gaoge). A microscope system was used to observe and record the three-phase microflow in microchannels, which included a high-speed CMOS camera (PL-A741, PixeLINK, working at 120 frames/s), an optical microscope (scale bar 0.008 mm/pixel, View Solutions), and a cold light source at bottom. Figure 1b shows the details of the double T-junction microchannel used in the experiment, which was fabricated on a polymethyl methacrylate (PMMA) plate using precision milling and sealed to a transparent chip using a high-pressure thermal sealing machine (A274, Techson) at 75°C and 0.4 MPa. In this chip, the straight main channel had a rectangular cross section with a width (w), height (h), and length (l) of 610 μm, 330 μm, and 40 mm, respectively. The side channels, which were used as the inlets of the dispersed phases, had the same height as the main channel but a smaller width (w_s) of 300 μm and shorter length (l_s) of 8 mm. The contact points of the two side channels on the main channel were 10 and 20 mm away from the continuous phase inlet. The microchannels were connected to Teflon pipes, which had an inner diameter of 520 μm. As the outlet pipe (38 cm) was much longer than the main channel (40 mm), the pressure drop in the chip was neglected for this relative low flow resistance. Using syringe pump to feed the gas phase will face the compressibility of gas phase, which might make deviations between the instant gas flow rates and the setting flow rates in the pump computer. Rectification of the gas flow rate was made in every test, which details are given in Appendix of this article.

Working systems and operation

An oil phase containing a high concentration of surfactant (n-octane solution with 2 wt % Span80) was used as the continuous phase in the experiment. The dispersed gas was air, and the dispersed liquids were chosen from deionized water (DI water) and two PEG 20,000 aqueous solutions with different concentrations. The fluid densities, viscosities, interfacial tensions (IFT) with oil and the contact angles (CA) on PMMA plate with oil as the bulk phase at the experimental temperature of 25°C are listed in Table 1. The Re numbers of three-phase fluids in their feeding channels are Re_O: 2.1–31.8; Re_G: 0.12–2.12; Re_O: 0.3–29.9. To simplify the terminology, the DI water is also called a 0 wt % PEG solution in the following figures. All the liquid and solid reagents were provided by Sinopharm Chemical Reagent Co., China. In every experimental test, the constant feeding sequence for the three-phase fluids was first gas, then oil, and finally water. After changing any operating condition, a stabilizing time of at least 1 min was allowed.

Data analysis

To characterize the final dispersed sizes of the bubbles and droplets, their average volumes ($V = Q/f$) were calculated from the fed flow rates (Q) of the dispersed phases and their generation frequencies (f) observed in recorded videos. These frequencies were obtained by counting the bubbles or droplets passing through the main channel for a constant recording time. The average volume of bubbles generated from junction T1 is represented by V_{G1}, and the average volumes of bubbles and droplets flowing in the downstream channel of junction T2 are represented by V_{G2} and V_{W2}, respectively, as shown in Figure 1c. Another two important parameters in the following discussion are the average volume of the droplets (V_W^*) generated without any disturbance from the cutting bubbles, which is called spontaneously generated droplet, and the average volume of the droplets used to cut the long gas slugs (V_W^{**}), which is called blocking droplet in this article. The average volume of spontaneously generated droplets ($V_W^* = Q_W \cdot t$) was obtained from the flow rate of the water phase (Q_W) and the average droplet generation time (t), which was determined from the microscope videos. The average volume of blocking droplets ($V_W^{**} = w \cdot h \cdot L_{BD}$) was directly calculated from the cross-section area of microchannel ($w \cdot h$) and the average length of blocking droplets (L_{BD}) for its cubic three-dimensional (3-D) shape as shown in Figure 1c. The lengths of all bubbles and droplets in the downstream microchannels of junction T2 were also measured from the videos, and they were used to characterize the size distributions. The polydispersity indexes (σ_{G1}, σ_{G2}, σ_{W2}), defined by Eqs. 1 and 2 were calculated, and showed the ratios of the standard deviations of the bubble/droplet lengths (l_{G1}, l_{G2}, l_{W2}) to the average bubble/droplet lengths (L_{G1}, L_{G2}, L_{W2})

$$\sigma_{G1,G2,W2} = \frac{1}{L_{G1,G2,W2}} \sqrt{\frac{1}{n-1} \sum \left(l_{G1,G2,W2} - L_{G1,G2,W2}\right)^2} \times 100\% \quad (1)$$

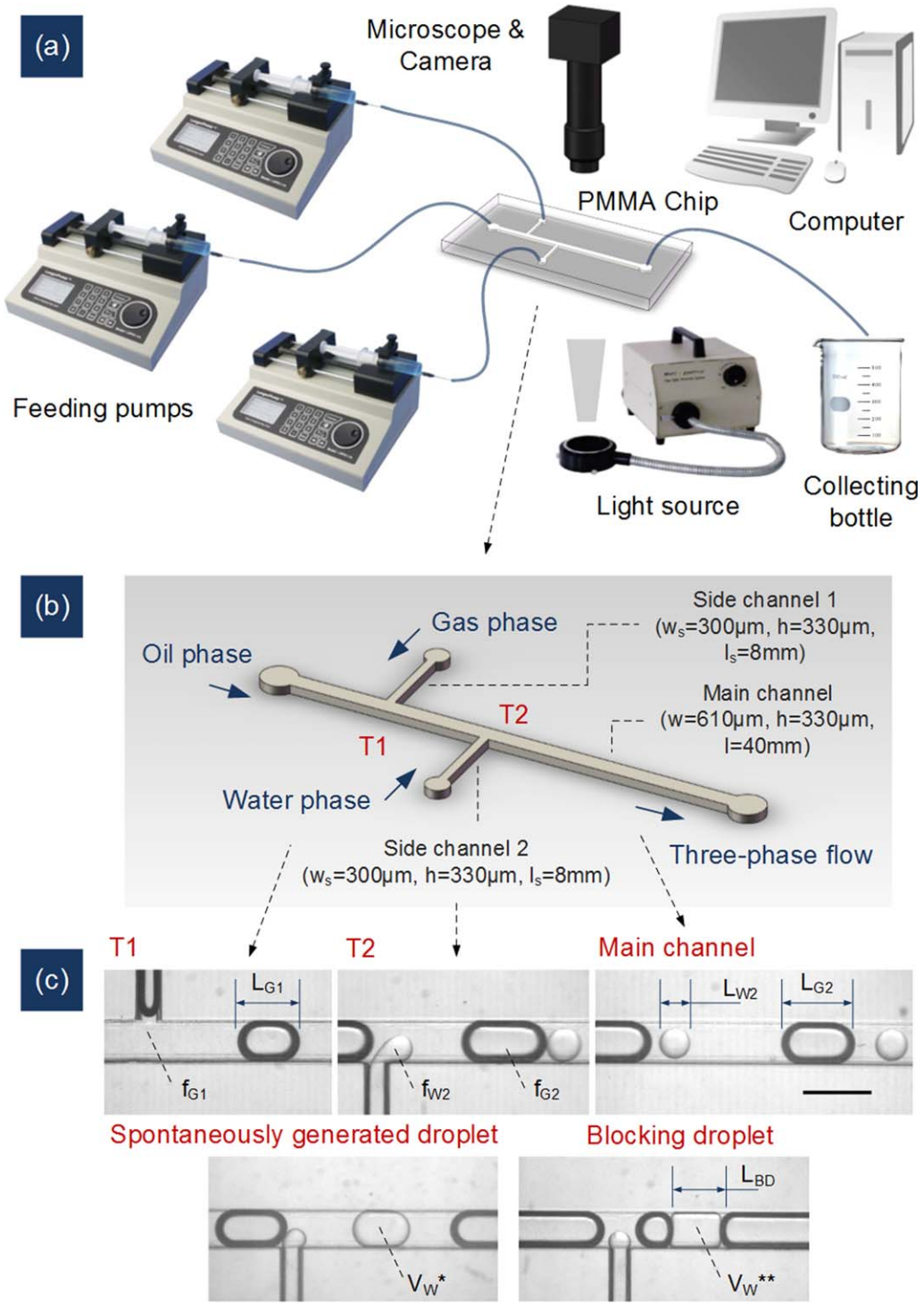

Figure 1. Schematic diagrams of the experimental platform and some important parameters: (a) the experimental setup, (b) the 3-D structure of microchannel, and (c) important parameters of bubbles and droplets.

[Color figure can be viewed in the online issue, which is available at wileyonlinelibrary.com.]

$$L_{G1,G2,W2}=\frac{1}{n}\sum_{1}^{n} l_{G1,G2,W2}, \quad 50 \le n \le 150 \qquad (2)$$

At least 50 bubbles or droplets were used to obtain the statistical values of the bubble and droplet generation frequencies, average bubble and droplet generation time, and polydispersity indexes of the bubble and droplet lengths.

Results and Discussion

Microbubbles generated in junction T1

We investigated the first bubble and second droplet generation sequence in this study. In junction T1, the gas phase was first dispersed in the oil phase. According to the experimental observation, all the bubbles were generated in the squeezing flow,[20] producing slug shaped bubbles, shown in

Table 1. Physical Properties of Working Systems[a] (25°C)

Phases	Fluids	Viscosities μ (mPa s)	Densities ρ (kg/m^3)	IFT with Oil γ (mN/m)	CA with Oil on PMMA, θ (°)
Oil	2 wt % Span80 *n*-octane solution	0.53	698	–	
Gas	Air	0.018	1	21.4	153
Water	DI water (0 wt % PEG solution)	0.89	997	3.53	146
	3 wt % PEG aqueous solution	2.12	998	3.40	149
	8 wt % PEG aqueous solution	8.74	998	3.69	144

[a]The densities of all liquids were measured with densitometers, and viscosities were measured with Ubbelohde viscometers. The IFT and the CA were measured with a tensiometer produced by DataPhysics Instruments GmbH. The model used to calculate the CA in the equipment software was ellipse method.

Figures 2a, b. Although the T-junction microchannel can also be used to prepare small and round bubbles at a high flow rate or high continuous phase viscosity, we did not select those operating conditions out of consideration for the weak bubble cutting effect and strong shearing force from the oil phase in junction T2.[16] Another reason that we only tested slug-shaped bubbles was the fact that the three-phase microflows were already complicated, and we needed to focus our experiment to provide a systematic discussion. The average lengths of the bubbles generated in the squeezing flow obeyed the simplest linear relation containing the flow rate ratio of the dispersed phase to the continuous phase (Q_G/Q_O).[21–23] Figure 2c shows the ratios of the average bubble length to channel width at different flow rate ratios, where the solid line represents Eq. 3, a formula correlated from our experimental results. As the volume of a slug shape bubble has an approximately linear relation with its length[21] and the cross-sectional area ($w{\cdot}h$) of the microchannel for a low-viscosity liquid, a characteristic volume w^2h has been already used to obtain a dimensionless dispersed phase volume in microfluidic literatures.[24,25] We overwrite the size law of bubbles to Eq. 4, which also agrees well with the experimental data, as shown in Figure 2d

$$L_{G1}/w = 0.85Q_G/Q_O + 1.25 \;;\; 0.05 < Q_G/Q_O < 10 \quad (3)$$

$$V_{G1}/w^2h = 0.85Q_G/Q_O + 0.88 \;;\; 0.05 < Q_G/Q_O < 10 \quad (4)$$

The polydispersity indexes of all generated bubbles (σ_{G1}) were less than 5%, showing their uniformity. More importantly, these monodispersed bubbles were generated at a

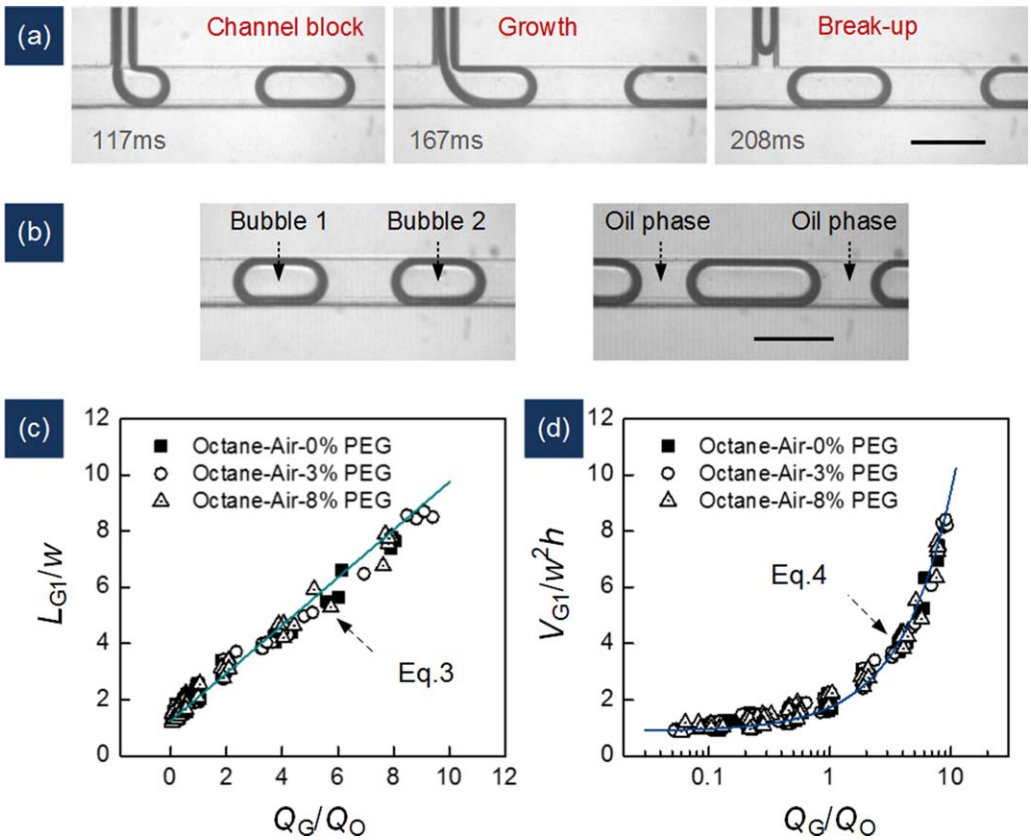

Figure 2. Bubble generation processes in junction T1 and their size law, with scale bar = 1 mm.

(a) Pictures of a bubble generation process (system: 2 wt % span80 octane solution/air/DI water, $Q_O = 100$ μL/min, $Q_G = 98$ μL/min, $Q_W = 100$ μL/min). (b) Bubbles in the straight microchannel after junction T1 (system: 2 wt % span80 octane solution/air/DI water; left: $Q_O = 400$ μL/min, $Q_G = 360$ μL/min, $Q_W = 200$ μL/min; right: $Q_O = 200$ μL/min, $Q_G = 371$ μL/min, $Q_W = 200$ μL/min). (c) Dimensionless average bubble lengths at different gas/oil flow rate ratios and the correlated line. (d) Dimensionless average bubble volumes at different gas/oil flow rate ratios and their correlated line. [Color figure can be viewed in the online issue, which is available at wileyonlinelibrary.com.]

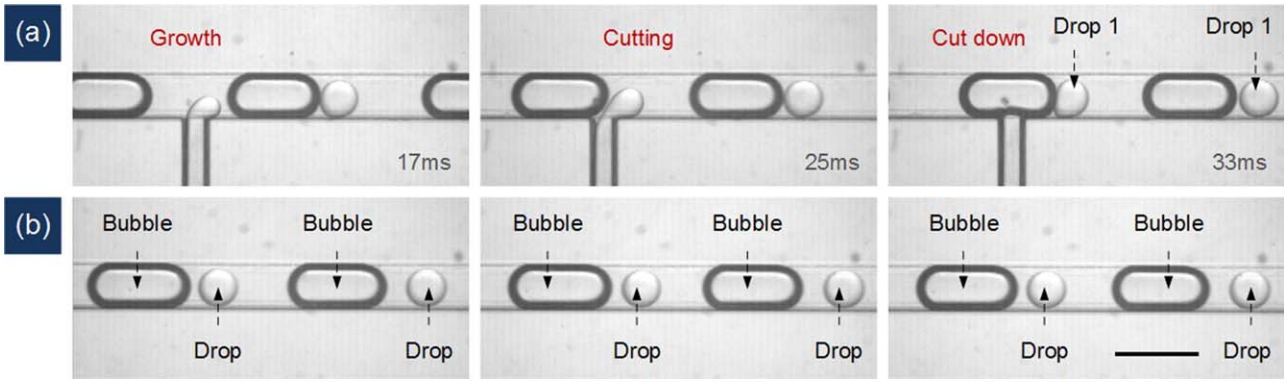

Figure 3. Images of a bubble cutting process and periodic three-phase flows in the main channel, with scale bar = 1 mm.

(a) Pictures of a bubble cutting process (system: 2 wt % span80 octane solution/air/3 wt % aqueous PEG solution, $Q_O = 400$ μL/min, $Q_G = 384$ μL/min, $Q_W = 100$ μL/min). (b) Periodic bubble/droplet alternate flow in the downstream microchannel of junction T2 [system is the same as Figure 3(a)]. [Color figure can be viewed in the online issue, which is available at wileyonlinelibrary.com.]

stable frequency, which can be represented by the ratio of the gas flow rate to the average bubble volume, as shown by Eq. 5

$$f_{G1} = Q_G / V_{G1} \tag{5}$$

Three-phase flow in junction T2

The bubbles generated in junction T1 had a very stable generation frequency, and we clearly observed their periodic cutting effect on the water phase in junction T2. This cutting effect came from the much higher continuous phase surface tension compared to the liquid/liquid interfacial tension. In this study, the surface tension of the oil phase was almost five times higher than the water/oil interfacial tension. Thus, the bubbles were much firmer, like a fully filled balloon, compared with the soft water phase in the confined microchannel. Different break-up phenomena of the water phase were observed during the experiment, and the simplest was called the "bubble cutting flow," as shown in Figure 3a. In this flow pattern, all the droplets were cut detached from the side channel. This cutting effect is useful in the preparation of small droplets. A stable three-phase flow with one droplet followed by one bubble was formed in the downstream microchannel, which is called "bubble/droplet alternate flow," as shown in Figure 3b. This flow pattern has potential for use in a particle preparation process such as for microbeads or microcapsules,[19] as the inert bubbles will prevent droplet coalescence in long-time polymerization or a crystallization process.[26] And, it can be also used in the flow chemistry process for the separated droplets are stable reacting units.[4] The droplet generation frequency (f_{W2}) in this flow pattern was equal to the bubble generation frequency in junction T1 (f_{G1}).

With an increase in the water phase flow rate, more than one droplet will be formed in a bubble cutting period, as shown by Figures 4a–c. In this situation, both the squeezing or shearing effect from the continuous phase and the cutting effect of the bubbles dominate the break-up of the water phase. Thus, the three-phase flow patterns become combinations of gas/liquid and liquid/liquid two-phase flow patterns. All the "spontaneous break-up processes" (representing droplet generation processes without disturbance from bubbles) in liquid/liquid microflows: squeezing,[21] dripping,[27] and jetting[28] flows, were investigated in the present work, instead of the single squeezing flow described in our previous report.[14] Squeezing flow and dripping flow were both observed at a low water phase flow rate or low water phase viscosity. The break-up points of these two flows were at the channel junction, and the standard we used to distinguish them was whether a growing droplet could block the main channel during its growth process. The squeezing flow only occurred when the main channel was entirely blocked. If the continuous phase passed the droplet at the moment of interface rupturing, the shearing effect from the continuous phase strongly affected the droplet generation.[29] Thus, the squeezing flow and dripping flow had different break-up mechanisms, and their droplet size laws were different. Jetting flow, in which the break-up point changes to the downstream channel of the T-junction, appeared at a medium flow rate and viscosity of the water phase in the experiment. In the jetting flow, the droplet break-up was dominated by the Rayleigh–Plateau instability of the interface.[30,31]

Figure 5 shows a flow map of all the "spontaneous break-up flows" in the bubble cutting interval. In this figure, the capillary number of the continuous phase, defined based on the oil/water interfacial tension (γ_{OW}), as shown by Eq. 6, is used for the x axis, representing the ratio of the viscous shearing force to the interfacial force. When the viscous shearing force is much lower than the interfacial force at $Ca_{OW} < 0.003$, the microchannel is easily blocked by the growing water phase, thus the flow pattern is squeezing flow. While, at higher Ca_{OW}, the growing droplet is hard to block the microchannel and the shearing force starts to become an important effect on the droplet generation process, which is the main character of a dripping flow. A similar transition point in a classical literature[21] was found. But according to other literatures, this transition point is not a constant value for different working systems and different structured microchannels.[32] The capillary number of water phase, defined by Eq. 7, is used for the y axis, representing the ratio of the viscous drag force in the water phase to the interfacial force and reflecting the difficulty of liquid phase break-up.[33] When the viscous drag force starts affecting the interfacial force at Ca_W equal to 0.01, the squeezing and dripping flows change to jetting flow

$$Ca_{OW} = \frac{\mu_O (Q_O + Q_G)}{w \cdot h \cdot \gamma_{OW}} \tag{6}$$

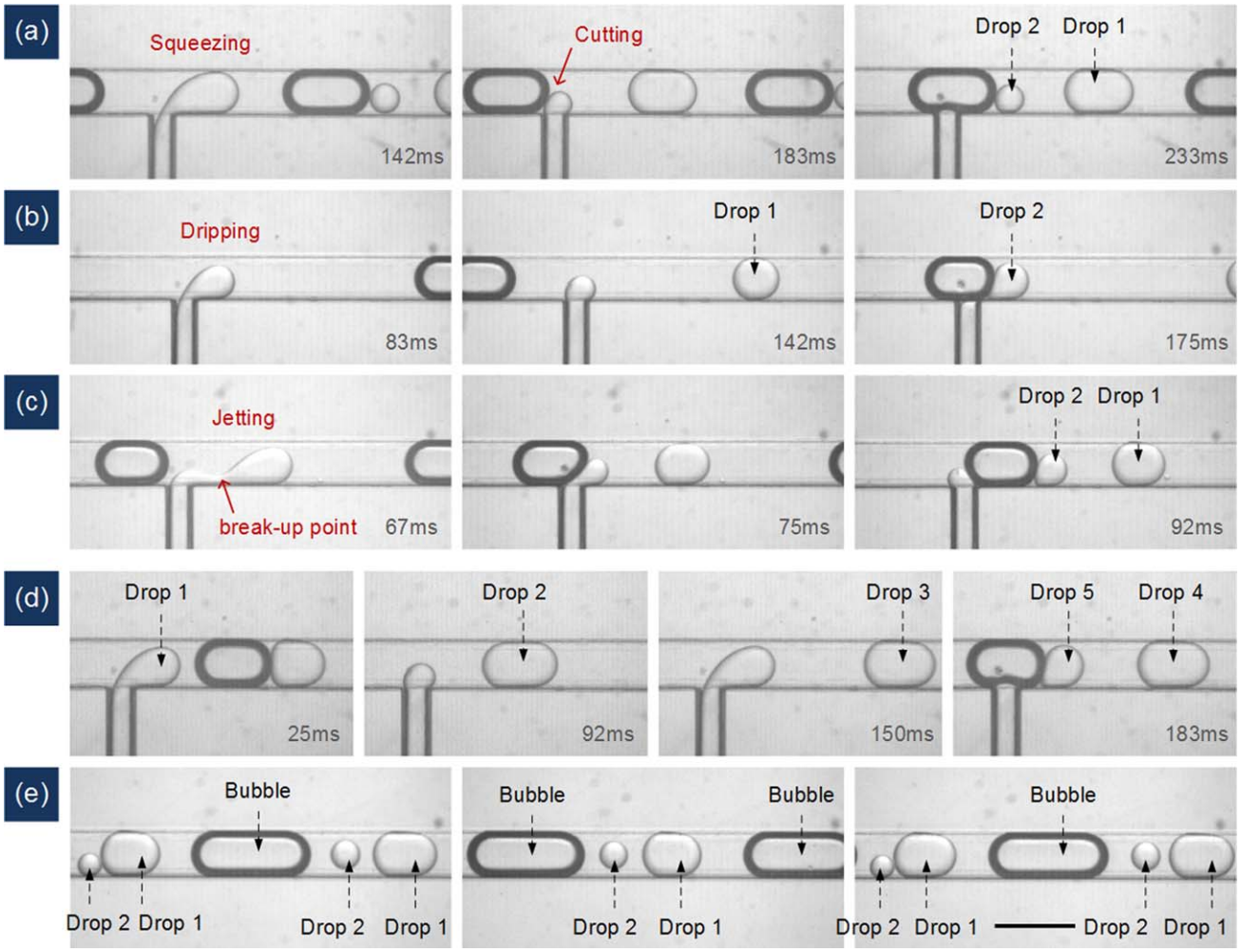

Figure 4. Different spontaneous break-up and bubble cutting coupling flows and formation of bubble/multidroplet alternate flow in the main channel, with scale bar = 1 mm.

(a) "Squeezing + bubble cutting flow" (system: 2 wt % span80 octane solution/air/DI water, $Q_O = 100$ μL/min, $Q_G = 51$ μL/min, $Q_W = 50$ μL/min). (b) "Dripping + bubble cutting flow" (system: 2 wt % span80 octane solution/air/3 wt % PEG aqueous solution, $Q_O = 400$ μL/min, $Q_G = 45$ μL/min, $Q_W = 50$ μL/min). (c) "Jetting + bubble cutting flow" (system: 2 wt % span80 octane solution/air/8 wt % PEG aqueous solution, $Q_O = 400$ μL/min, $Q_G = 121$ μL/min, $Q_W = 100$ μL/min). (d) Formation of five droplets in a bubble cutting period (system: 2 wt % span80 octane solution/air/DI water, $Q_O = 400$ μL/min, $Q_G = 53$ μL/min, $Q_W = 200$ μL/min). (e) Bubble/multidroplet alternate flow in the main channel after junction T2 (system: 2 wt % span80 octane solution/air/DI water, $Q_O = 200$ μL/min, $Q_G = 183$ μL/min, $Q_W = 100$ μL/min). [Color figure can be viewed in the online issue, which is available at wileyonlinelibrary.com.]

$$\mathrm{Ca_W} = \frac{\mu_W Q_W}{w_S \cdot h \cdot \gamma_{OW}} \tag{7}$$

To simplify the analysis, the transition region between different flow patterns was not considered in this study. For example, the transition flow from squeezing to dripping[25] was incorporated into the dripping flow in this article, which makes the distinction seem arbitrary. Fortunately, this crude partition fits with the experimental data, and we do not exclude the idea of conducting a more detailed analysis of the spontaneous droplet generation process to obtain more accurate model results.

In the analysis of the experiment, we found that the main reason for the appearance of the spontaneous droplet break-up was the bubble cutting frequency (f_{G1}) becoming lower than the spontaneous droplet generation frequency in theory ($f^*_{W2} = Q_W/V^*_W$). Therefore, more than one droplet could be formed in a bubble cutting period, and we observed this in our experiment when five droplets were followed by one bubble, as shown in Figure 4d. Because of the insufficient growth of the last droplet, it was always smaller in size. The good news was that all the earlier droplets had nearly the same volume, which was helpful for the analysis of the size law. Figure 4e shows the three-phase flow patterns in the main channel, which is called "bubble/multidroplet alternate flow" in this article. Although this flow pattern cannot provide uniform droplets, it is still useful in multiphase chemical reactions, because the plug flow can provide a narrow residence time for reactants.[34]

According to the previous two-phase flow study in the T-junction microchannel, the nondispersed liquid/liquid parallel flow will appear at higher viscosity and flow rate of the dispersed phase,[35] where the viscous drag force meets the interfacial force. Figure 5 shows its possible appearance region ($0.04 < \mathrm{Ca_W} < 0.2$) in this study based on our estimation (this estimation assumed that the parallel flow occurred

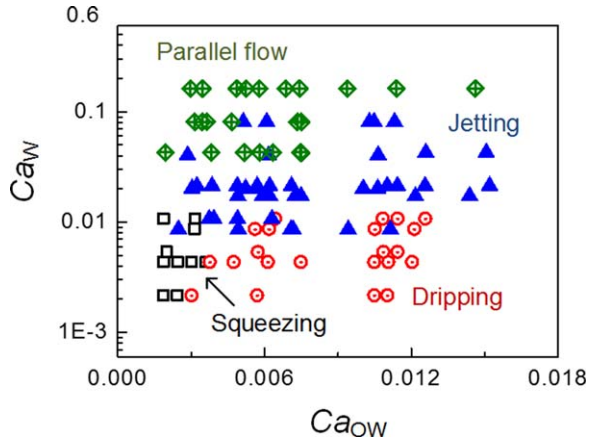

Figure 5. Flow map of liquid/liquid squeezing, dripping, jetting, and nondispersed parallel flows in the bubble cutting interval.

[Color figure can be viewed in the online issue, which is available at wileyonlinelibrary.com.]

when there was no spontaneous droplet break-up at a relatively high Ca_W). This estimation was used because all the parallel flows were disturbed by the bubbles. Therefore, no stable parallel flow was observed during the experiment. We found that the bubbles had a strong cutting ability in the confined microchannel. Although the most viscous PEG aqueous solution ($\mu_W = 8.74$ mPa s) was hard to break in the cross-flow direction, the bubble still split it in the perpendicular direction, as shown in Figure 6a. This flow pattern transition from parallel flow to segment flow with the help of gas phase is benefit for the mass-transfer enhancement between liquid/liquid phases containing high viscous fluids. The flow pattern in the main channel was still a bubble/droplet alternate flow, but the droplets always had a long plug shape, as shown in Figure 6b. An interesting phenomenon was that some of the droplets were not full of the channel section. This should have been because of the high viscosity of the water phase, which caused the interface to shrink slowly, and the fact that some continuous phase was blocked beside the droplet.

In addition to the "bubble cutting flow" and "spontaneous break-up and bubble cutting coupling flow," the last flow pattern we observed at junction T2 is called the "bubble/droplet alternate break-up flow." This phenomenon only appeared in the tests with long gas slugs, as shown in Figure 7. In this flow, the gas slugs were broken when passing the side channel under a perpendicular squeezing effect from the water phase. Because of the alternate break-up processes of the gas phase and water phase, the generated flow pattern was also a bubble/droplet alternate flow and the embedded droplets (Drop 2) have a cubic shape due to the less continuous phase around them, as shown in Figure 7c. However, the alternate break-up process caused nonuniform bubbles and droplets, which had polydispersity higher than 7%.

A simple criterion to determine whether the alternate bubble/droplet cutting process occurs is summarized based on the experiment. First, the bubble length should be more than three times the channel width, otherwise the gas slug cannot block the main channel on both sides of the side channel, which is similar as the droplet break-up process in the branch microchannels.[36,37] Second, the bubble passage time through junction T2 should be larger than its break-up time (t_b). This criterion is described as follows

$$L_{G1}/w > 3 \tag{8}$$

$$\frac{(L_{G1}-w_s)}{u_G} \approx \frac{(L_{G1}-w_s)wh}{(Q_G+Q_O)} > t_b \tag{9}$$

where u_G is the bubble moving speed, which was considered to the total flow rate of the gas and oil phases. As the bubble break-up is caused by the insertion of water phase, its time can be evaluated by the volume of blocking droplet and the feeding flow rate of water phase ($t_b \approx V_W^{**}/Q_W$). As shown in Figures 7a, b, an arch-shaped water phase is stored in one side of the bubble, growing quickly with the feeding of water phase. The driving force of bubble break-up process is the squeezing force from water phase coming out of the perpendicular side channel and the resistance force is the interfacial force of both gas/oil and water/oil interfaces. At high flow rate of water phase, which means the squeezing force of water phase is strong, the bubble break-up time is shortened, but the blocking droplet volume was found increase with the rising of water flow rate. The reason is the increased inertia force of

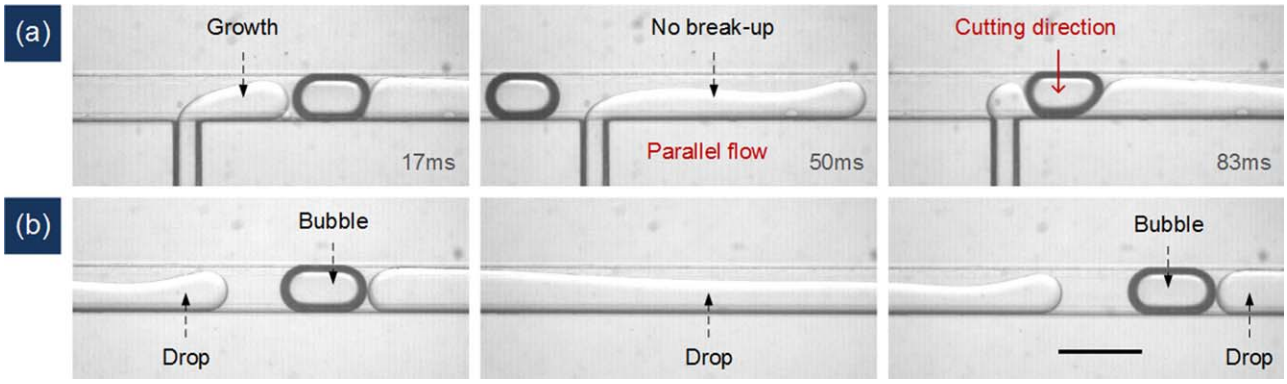

Figure 6. Bubble cutting process in theoretical liquid/liquid parallel flow and three-phase flow in the main channel, with scale bar = 1 mm.

(a) Bubble cutting process (system: 2 wt % span80 octane solution/air/8 wt % PEG aqueous solution, $Q_O = 400$ μL/min, $Q_G = 88$ μL/min, $Q_W = 400$ μL/min). (b) Bubble/droplet alternate flow in the main channel after junction T2. The images were captured at the same location but different time to exhibit the entire flow pattern. (System: 2 wt % span80 octane solution/air/8 wt % PEG aqueous solution, $Q_O = 200$ μL/min, $Q_G = 66$ μL/min, $Q_W = 400$ μL/min). [Color figure can be viewed in the online issue, which is available at wileyonlinelibrary.com.]

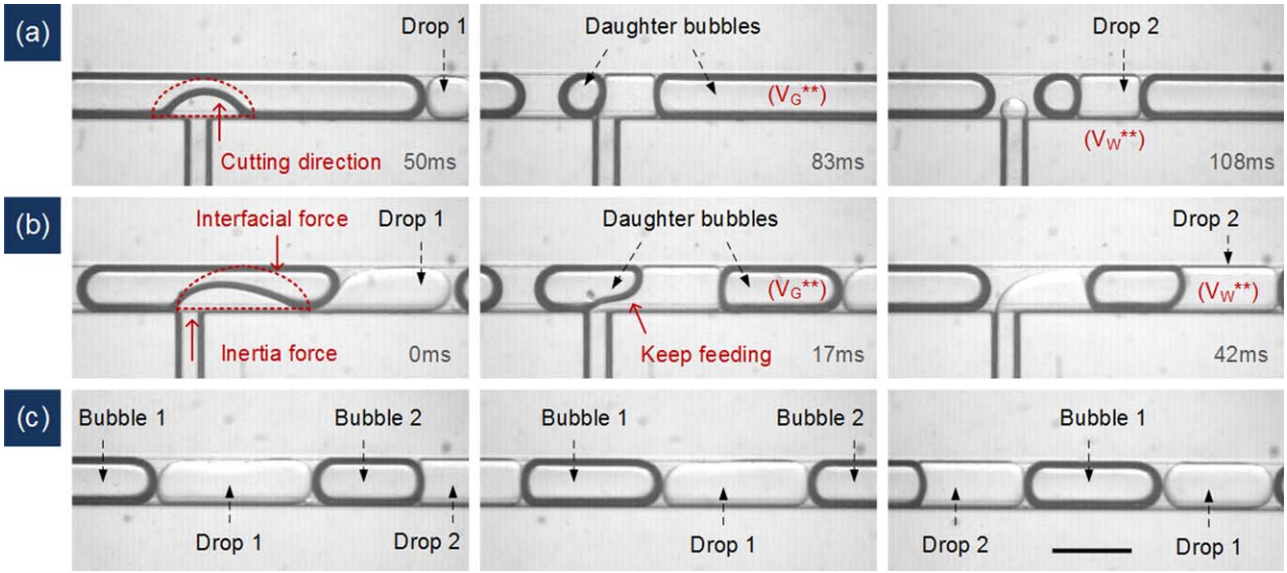

Figure 7. Bubble/droplet alternate cutting process and formation of three-phase microflow, with scale bar = 1 mm.

(a) Long bubble break-up under the cutting of the water phase (system: 2 wt % span80 octane solution/air/DI water, $Q_O = 50$ μL/min, $Q_G = 398$ μL/min, $Q_W = 100$ μL/min). (b) Bubble break-up at a higher water phase flow rate (system: 2 wt % span80 octane solution/air/8 wt % PEG aqueous solution, $Q_O = 100$ μL/min, $Q_G = 396$ μL/min, $Q_W = 400$ μL/min). (c) Bubble/ droplet alternate flow in the main channel (under the same operating conditions as Figure 7b). [Color figure can be viewed in the online issue, which is available at wileyonlinelibrary.com.]

water phase in the side channel quickly changes its direction after coming to the main channel, making the blocking droplet shape flatter under the confinement of interfaces. This phenomenon is shown in Figures 7a, b. A modified Webber number is defined to characterize growing of blocking droplet volume as shown by Eq. 10

$$We'_W = \frac{\rho_W Q_W^2 d e_s}{w_s^2 h^2 (\gamma_{OW} + \gamma_{OG})} \tag{10}$$

The values of this modified Webber number were verified from 3.6×10^{-3} to 9.6×10^{-2} in the experiment, and the results exhibited the dimensionless V_W^{**}/w^2h also known as the dimensionless droplet length (L_{BD}/w) nearly had a linear

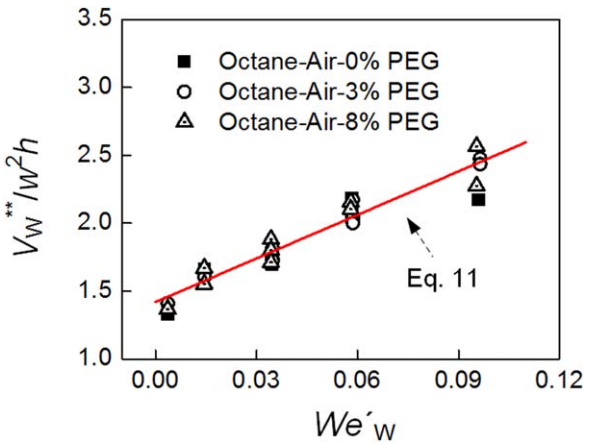

Figure 8. Relation of dimensionless average volume of blocking droplets and Webber number of water phase.

The points represents different gas and oil flow rates ($Q_G = 182$–512 μL/min, $Q_O = 50$–125 μL/min), and the different viscosities of the water phases. [Color figure can be viewed in the online issue, which is available at wileyonlinelibrary.com.]

relation with We'_W for all the working systems in the present study, as shown in Figure 8

$$V_W^{**}/w^2h = L_{BD}/w = 10.7We'_W + 1.42;\ We'_W \le 0.096 \tag{11}$$

Thus, the value of t_b in Eq. 9 can be evaluated using Eq. 11. In Eq. 11, the constant 1.42 is the smallest dimensionless droplet length required to break the bubble as We'_W moves toward infinite. The shearing gas phase passing the water phase had a similar effect to flat the water plug, however, it was not obvious for the low viscous force of gas ($\mu_G/\mu_W < 0.02$). Therefore, the flow rate of gas/oil two phases had little effect. The effect of water-phase viscosity was not obvious either, because of the relative lower vicious force of water phase comparing with its inertia force. A new capillary number of water phase like the modified Webber number was defined and the results show this Ca'_w are ranged from 6.1×10^{-4} to 3.1×10^{-2}, which are smaller than the We'_W

$$Ca'_W = \frac{\mu_W Q_W}{w_s h (\gamma_{OW} + \gamma_{OG})} \tag{12}$$

Size laws of final bubbles and droplets

The systematic analysis of the bubble and droplet generation mechanism described in the above sections is important to determine their size laws for these complicated three-phase flows. The simplest size law for the generated droplets involves the bubble cutting flow for an equal number of final bubbles to droplets. As the droplet generation frequency in junction T2 (f_{W2}) is equal to the bubble generation frequency in junction T1 (f_{G1}), their average volumes are easily given as follows

$$\frac{V_{W2}}{w^2h} = \frac{Q_W}{w^2h \cdot f_{G1}} = \frac{Q_W}{Q_G} \cdot \left(0.85\frac{Q_G}{Q_O} + 0.88\right) \tag{13}$$

Equation 13 has good accuracy, as shown in Figure 9. Few separated points exist due to the experimental errors.

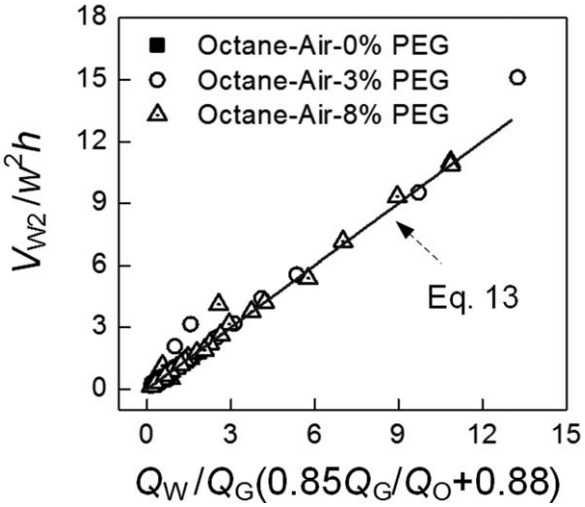

Figure 9. Dimensionless average volumes of droplets generated in the bubble cutting flow.

For the mixing flows of the bubble cutting and the spontaneous break-up processes, we should first determine the size laws for the spontaneously generated droplets. Several previous studies have provided droplet volume or droplet diameter models based on theoretical analyses[27] or semiempirical correlations.[29] In this article we choose the semiempirical models because of their relatively high accuracy in volume prediction, which is important for the accuracy of further models. The semiempirical models also have the advantage of simplified calculations, which are suitable for application. In the squeezing flow, the average droplet volume (V_W^*) has the same size law as the gas/liquid squeezing flow, satisfying a linear relation with the flow rate ratio, as shown by Eq. 14

$$\frac{V_W^*}{w^2h}=0.85\frac{Q_W}{Q_O+Q_G}+0.88;\quad \frac{Q_W}{Q_O+Q_G}<1 \tag{14}$$

In the dripping flow, the average droplet volume is in accord with a function of the flow rate ratio and capillary number, because the squeezing and shearing effects from the continuous phase work together.[38] Equation 15 gives the correlated formula based on the present experiment

$$\frac{V_W^*}{w^2h}=0.58\left(\frac{Q_W}{Q_O+Q_G}\right)^{0.44}\mathrm{Ca_{OW}}^{-0.19};\quad \frac{Q_W}{Q_O+Q_G}<0.5,\mathrm{Ca_{OW}}<0.016 \tag{15}$$

For the liquid/liquid jetting flow, the interface break-up occurs, because of the Rayleigh–Plateau effect. Previous work has proven that the relative droplet size in jetting flow is an exponential function of the flow rate ratio.[39] Using this relation, the droplet volumes in the spontaneous jetting flow are given by Eq. 16

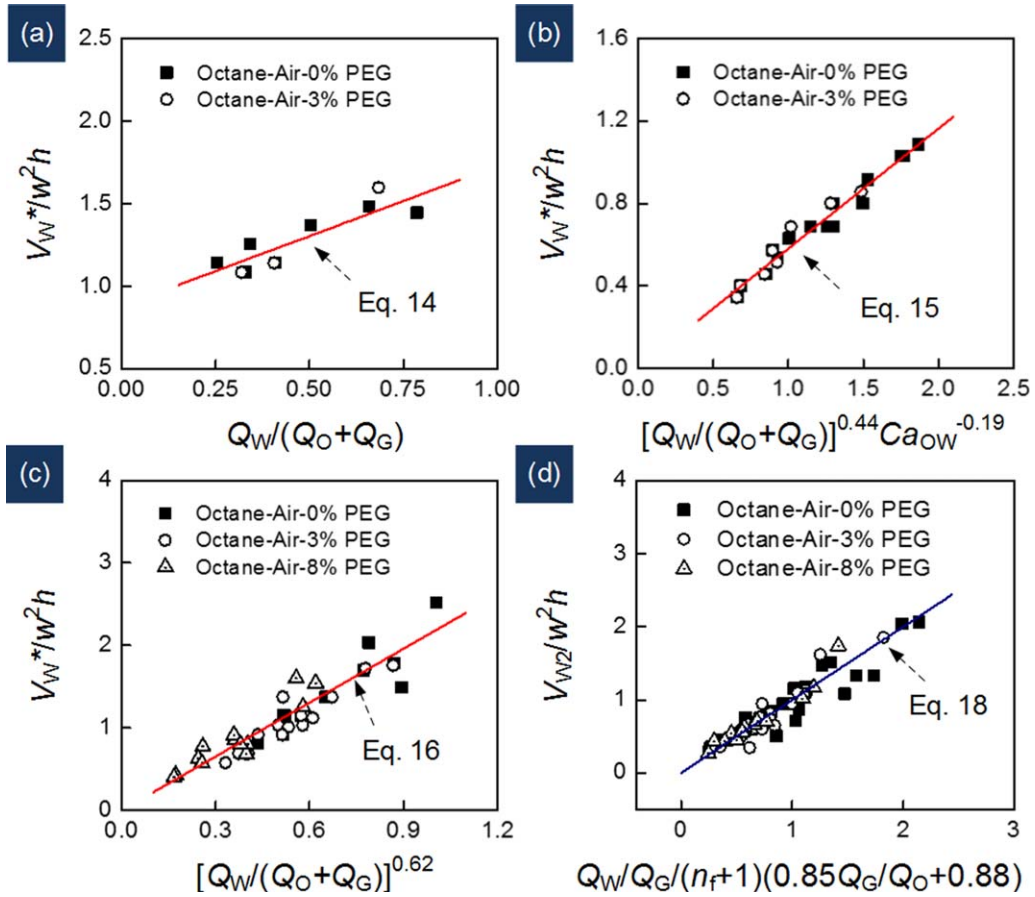

Figure 10. Dimensionless average volumes of the spontaneously generated droplets and the final droplets: (a) droplets generated in squeezing flow, (b) dripping flow, (c) jetting flow, and (d) all droplets.

[Color figure can be viewed in the online issue, which is available at wileyonlinelibrary.com.]

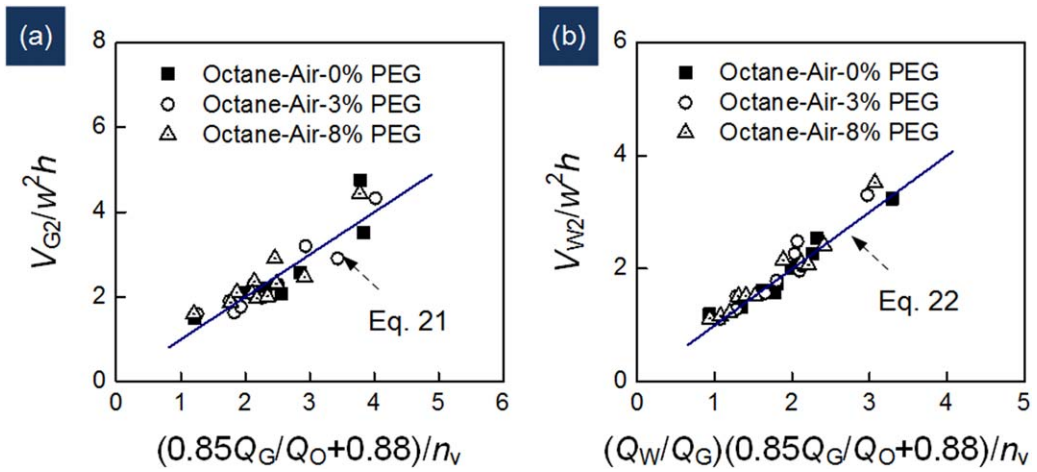

Figure 11. Dimensionless average volumes of bubbles and droplets from alternate break-up flows: (a) dimensionless average volumes of bubbles generated in junction T2 and (b) dimensionless average volumes of droplets generated in junction T2 and their correlated line.

[Color figure can be viewed in the online issue, which is available at wileyonlinelibrary.com.]

$$\frac{V_W^*}{w^2h}=2.2\left(\frac{Q_W}{Q_O+Q_G}\right)^{0.62};\quad \frac{Q_W}{Q_O+Q_G}<1.5 \tag{16}$$

Figures 10a–c shows comparisons of the experimental data and results of the correlated equations, showing low deviations. Using these equations, the theoretical generation frequency of spontaneous generated droplet is calculated as $f_W^*=Q_W/V_W^*$. When this frequency is higher than the bubble cutting frequency f_{G1}, more than one droplets will formed in a cutting period, and the actual generation frequency of all the droplets in junction T2 can be represented by ratio function of f_W^* to f_{G1}, shown in Eq. 17

$$f_{W2}=f_{G1}(n_f+1)=f_{G1}\cdot\left[\mathrm{Int}\left(f_W^*/f_{G1}\right)+1\right] \tag{17}$$

where n_f is the integer value of frequency ratio f_W^*/f_{G1}. Based on the calculated generation frequency in Eq. 16, the average droplet volumes are finally given by Eq. 18, and the model and experimental results are shown in Figure 10d

$$\frac{V_{W2}}{w^2h}=\frac{Q_W}{w^2h\cdot f_{G1}(n_f+1)}=\frac{Q_W}{Q_G(n_f+1)}\left(0.85\frac{Q_G}{Q_O}+0.88\right) \tag{18}$$

In the last flow pattern, the bubble/droplet alternate break-up flow, we have given the size law of blocking droplets (V_W^{**}) at junction T2 in Eq. 11. Considering the blocking droplets and the daughter bubbles at the downstream channel of junction T2 (labeled by V_G^{**} in Figure 7) were alternately generated, their average volume ratio is equal to the feeding flow rate ratio, given by Eq. 19

$$\frac{V_G^{**}}{w^2h}=\frac{V_W^{**}}{w^2h}\frac{Q_G+Q_O}{Q_W} \tag{19}$$

Thus, the number of the daughter bubbles for an original bubble from junction T1 is

$$n_v=\mathrm{Int}\left(V_{G1}/V_{G1}^{**}\right)+1 \tag{20}$$

and the bubble/droplet generation frequency in junction T2 ($f_{G2}=f_{W2}$) is $n_v f_{G1}$. Using this equation, the final bubble and

Table 2. Summary of Main Results in the Present Work

Flow Pattern at Junction T2	Operating Criteria	Flow Patterns in Main Channel	Polydispersity Index Levels[a]	Average Volumes
Bubble cutting flow	$f_w^*<f_{G1}$	Bubble/droplet alternate flow	$\sigma_{G1}=\sigma_{G2}<5\%$	Eq. 13
Squeezing + bubble cutting flow	$f_w^*>f_{G1}$ $Ca_{OW}<0.003$ $Ca_W<0.01$	Bubble/multidropl et al ternate flow	$\sigma_{G1}=\sigma_{G2}<5\%$ $\sigma_{W2}>5\%$	Eq. 4 Eq. 14 Eq. 18
Dripping + bubble cutting flow	$f_w^*<f_{G1}$ $Ca_{OW}>0.003$ $Ca_W<0.01$	Bubble/multidropl et al ternate flow	$\sigma_{G1}=\sigma_{G2}<5\%$ $\sigma_{W2}>5\%$	Eq. 4 Eq. 15 Eq. 18
Jetting + bubble cutting flow	$f_w^*>f_{G1}$ $0.01<Ca_W<0.1$	Bubble/multidropl et al ternate flow	$\sigma_{G1}=\sigma_{G2}<5\%$ $\sigma_{W2}>5\%$	Eq. 4 Eq. 16 Eq. 18
Bubble/droplet alternate break-up flow	$L_{G1}>3w$ $(L_{G1}-w_s)/u_G>t_b$	Bubble/dropl et al ternate flow	$\sigma_{G1}<5\%$ $\sigma_{G2}>5\%$ $\sigma_{W2}>5\%$	Eq. 21 Eq. 22

[a]A polydispersity index lower than 5% means the droplets or bubbles are monodispersed, otherwise the droplets or bubbles are polydispersed.

droplet volumes are given by Eqs. 21 and 22, respectively. The experimental data shown in Figure 11 agree well with the results of these equations

$$\frac{V_{G2}}{w^2h}=\frac{V_{G1}}{n_v w^2 h}=\frac{1}{n_v}\left(0.85\frac{Q_G}{Q_O}+0.88\right) \tag{21}$$

$$\frac{V_{W2}}{w^2h}=\frac{V_{G1}}{n_v w^2 h}\cdot\frac{Q_W}{Q_G}=\frac{Q_W}{n_v Q_G}\left(0.85\frac{Q_G}{Q_O}+0.88\right) \tag{22}$$

Based on the above analysis, a model used to calculate all the average bubble/droplet volumes in this experimental study can be written as follows

$$\begin{cases} V_{G2}=Q_G/f_{G2}=Q_G {f_{G1}}^{-1} {n_v}^{-1} \\ V_{W2}=Q_W/f_{W2}=Q_W {f_{G1}}^{-1}\left(n_v+n_f\right)^{-1} \end{cases} \tag{23}$$

Conclusion

The generation of gas/liquid/liquid three-phase microflows and bubble/droplet size laws for a double T-junction microchannel was introduced. At the first T-junction, slug-shaped bubbles were controllably prepared from a gas/oil squeezing flow, providing a periodic cutting effect on the water phase at the second T-junction. The three-phase microflows were formed with three flow patterns: bubble cutting flow, spontaneous break-up and bubble cutting coupling flow, and bubble/droplet alternate break-up flow. Among these flow patterns, the bubble cutting flow had the simplest generation mechanism, forming a flow with alternating bubbles and droplets in the main channel. The spontaneous break-up and bubble cutting coupling flow had the most complicated flow phenomena, containing squeezing, dripping, and jetting daughter flows, which finally produced bubble/multidroplet flow in the main channel. In the bubble/droplet alternate break-up flow, gas slugs were secondarily dispersed by the water phase, and this break-up process produced nonuniform daughter bubbles and droplets. All these break-up phenomena, flow patterns, and their criteria for the present experiment are listed in Table 2. The average volumes of bubbles and droplets were established based on the pervious published correlations for the gas/liquid and liquid/liquid two-phase systems, which fit well with the experimental data. Considering the complexity of three-phase systems, further works will be in-depth conducted in our research, such as the pressure drops in different flow patterns, which are important for the energy analysis of microflow process.

Acknowledgment

The authors like to acknowledge the supports from the National Natural Science Foundation of China (21106076, U1302271, 91334201), and the National Excellent Doctoral Dissertation Author Foundation of China (FANEDD 201349) on this work.

Notation

Ca_{OW} = capillary number of oil phase based on oil/water interfacial tension, $[Ca_{OW}=\mu_O(Q_O+Q_G)/wh\gamma_{OW}]$
Ca_W = capillary number of water phase $[Ca_W=\mu_W Q_W/w_s h\gamma_{OW}]$
Ca'_W = modified Capillary number of water phase, $[Ca'_W=\mu_W Q_W/w_s h(\gamma_{OW}+\gamma_{OG})]$
d_{G1} = average gas disk diameter in the monitor chamber, m
de = hydrodynamic diameter of the main channel, $[de=2wh/(w+h)]$, m
de_s = hydrodynamic diameter of the side channel, $[de_s=2w_s h/(w_s+h)]$, m
f = bubble/droplet generation frequency, s^{-1}
f_{G1} = bubble generation frequency in junction T1, s^{-1}
f_{G2} = bubble generation frequency in junction T2, s^{-1}
f_{W2} = droplet generation frequency in junction T2, s^{-1}
f_W^* = generation frequency of spontaneously generated droplet, s^{-1}
H = monitor chamber height, m
h = microchannel height, m
L_{BD} = average length of blocking droplet, m
L_{G1} = average bubble length in main channel after junction T1, m
L_{G2} = average bubble length in main channel after junction T2, m
L_{W2} = average droplet length in main channel after junction T2, m
l = main channel length, m
l_{BD} = separate length of blocking droplet, m
l_{G1} = separate bubble length in main channel after junction T1, m
l_{G2} = separate bubble length in main channel after junction T2, m
l_s = side channel length, m
l_{W2} = separate droplet length in main channel after junction T2, m
n = sample numbers
n_f = integer value of generation frequency ratio, $[n_f=f_W^*/f_{G1}]$
n_v = number of daughter droplets, $[n_v=\mathrm{Int}(V_{G1}/V_G^{**})+1]$
Q = flow rate, m^3/s
Q_G = gas-phase flow rate, m^3/s
Q_O = oil-phase flow rate, m^3/s
Q_W = water-phase flow rate, m^3/s
Re_G = Reynolds number of gas phase, $[Re_G=de_s\rho_G Q_G/w_s h\mu_G]$
Re_O = Reynolds number of oil phase, $[Re_O=de\rho_O Q_O/wh\mu_O]$
Re_W = Reynolds number of water phase, $[Re_W=de_s\rho_W Q_W/w_s h\mu_W]$
t = bubble/droplet generation time, s
t_b = bubble break-up time, s
V = average volume of bubbles or droplets, m^3
V_{G1} = average bubble volume in main channel after junction T1, m^3
V_{G2} = average bubble volume in main channel after junction T2, m^3
V_{W2} = average droplet volume in main channel after junction T2, m^3
V_W^* = average volume of spontaneously generated droplets, m^3
V_W^{**} = average volume of blocking droplets, m^3
V_G^{**} = average volume of daughter bubbles generated by the squeezing from blocking droplets, m^3
We'_W = modified Webber number of water phase $[We'_W=de_s\rho_W Q_W^2/w_s^2 h^2(\gamma_{OW}+\gamma_{OG})]$
w = main channel width, m
w_s = side channel width, m
σ_{G1} = length polydispersity index of bubbles generated from T1, %
σ_{G2} = length polydispersity index of bubbles generated from T2, %
σ_{W2} = length polydispersity index of droplets generated from T2, %
μ_G = viscosity of gas phase, Pa s
μ_O = viscosity of oil phase, Pa s
μ_W = viscosity of water phase, Pa s
ρ_G = density of gas phase, kg/m^3
ρ_O = density of oil phase, kg/m^3
ρ_W = density of water phase, kg/m^3
γ_{OG} = surface tension of oil phase in air, N/m
γ_{OW} = interfacial tension between water and oil phase, N/m

Literature Cited

1. Nisisako T, Okushima S, Torii T. Controlled formulation of monodisperse double emulsions in a multiple-phase microfluidic system. *Soft Matter*. 2005;1:23–27.
2. Wang K, Qin K, Wang T, Luo GS. Ultra-thin liquid film extraction based on a gas-liquid-liquid double emulsion in a microchannel device. *RSC Adv*. 2015;5:6470–6474.
3. Zheng B, Ismagilov RF. A microfluidic approach for screening submicroliter volumes against multiple reagents by using preformed arrays of nanoliter plugs in a three-phase liquid/liquid/gas flow. *Angew Chem Int Ed*. 2005;44:2520–2523.
4. Nightingale AM, Phillips TW, Bannock JH, de Mello JC. Controlled multistep synthesis in a three-phase droplet reactor. *Nat Commun*. 2014;5:3777.
5. Onal Y, Lucas M, Claus P. Application of a capillary microreactor for selective hydrogenation of α,β-unsaturated aldehydes in aqueous multiphase catalysis. *Chem Eng Technol*. 2005;28:972–978.
6. Assmann N, von Rohr PR. Extraction in microreactors: intensification by adding an inert gas phase. *Chem Eng Process*. 2011;50:822–827.

7. Tan J, Dong C, Lu YC, Xu JH, Luo GS. Coupling process of oxidation and extraction in a gas-liquid-liquid microdispersion system for H_2O_2 synthesis. *Ind Eng Chem Res*. 2012;51:1834–1845.
8. Wan J, Bick A, Sullivan M, Stone HA. Controllable microfluidic production of microbubbles in water-in-oil emulsions and the formation of porous microparticles. *Adv Mater*. 2008;20:3314–3318.
9. Chen R, Dong PF, Xu JH, Wang YD, Luo GS. Controllable microfluidic production of gas-in-oil-in-water emulsions for hollow microspheres with thin polymer shells. *Lab Chip*. 2012;12:3858–3860.
10. Shui LL, Eijkel J, van den Berg A. Multiphase flow in micro- and nanochannels. *Sens Actuat B Chem*. 2007;121:263–276.
11. Zhao CX, Middelberg A. Two-phase microfluidic flows. *Chem Eng Sci*. 2011;66:1394–1411.
12. Yue J, Rebrov EV, Schouten JC. Gas-liquid-liquid three-phase flow pattern and pressure drop in a microfluidic chip: similarities with gas-liquid/liquid-liquid flows. *Lab Chip*. 2014;14:1632–1649.
13. Su YH, Chen GW, Zhao YC, Yuan Q. Intensification of liquid-liquid two-phase mass transfer by gas agitation in a microchannel. *AIChE J*. 2009;55:1948–1958.
14. Wang K, Lu YC, Tan J, Yang BD, Luo GS. Generating gas/liquid/liquid three-phase microdispersed systems in double T-junctions microfluidic device. *Microfluid Nanofluid*. 2010;8:813–821.
15. Khan SA, Duraiswamy S. Microfluidic emulsions with dynamic compound drops. *Lab Chip*. 2009;9:1840–1842.
16. Rajesh VM, Buwa VV. Experimental characterization of gas-liquid-liquid flows in T-junction microchannels. *Chem Eng J*. 2012;207:832–844.
17. Hashimoto M, Garstecki P, Whitesides GM. Synthesis of composite emulsions and complex foams with the use of microfluidic flow-focusing devices. *Small*. 2007;3:1792–1802.
18. Xu JH, Chen R, Wang YD, Luo GS. Controllable gas/liquid/liquid double emulsions in a dual-coaxial microfluidic device. *Lab Chip*. 2012;12:2029–2036.
19. Abate AR, Weitz DA. Air-bubble-triggered drop formation in microfluidics. *Lab Chip*. 2011;11:1713–1716.
20. De Menech M, Garstecki P, Jousse F, Stone HA. Transition from squeezing to dripping in a microfluidic T-shaped junction. *J Fluid Mech*. 2008;595:141–161.
21. Garstecki P, Fuerstman MJ, Stone HA, Whitesides GM. Formation of droplets and bubbles in a microfluidic T-junction – scaling and mechanism of break-up. *Lab Chip*. 2006;6:437–446.
22. Van Steijn V, Kreutzer MT, Kleijn CR. mu-PIV study of the formation of segmented flow in microfluidic T-junctions. *Chem Eng Sci*. 2007;62:7505–7514.
23. Fu T, Ma Y, Funfschilling D, Zhu C, Li HZ. Squeezing-to-dripping transition for bubble formation in a microfluidic T-junction. *Chem Eng Sci*. 2010;65:3739–3748.
24. Van Steijn V, Kleijn CR, Kreutzer MT. Predictive model for the size of bubbles and droplets created in microfluidic T-junctions. *Lab Chip*. 2010;10:2513–2518.
25. Glawdel T, Elbuken C, Ren CL. Droplet formation in microfluidic T-junction generators operating in the transitional regime. I. Experimental observations. *Phys Rev E*. 2012;85:016322.
26. Chen D, Li L, Reyes S, Adamson DN, Ismagilov RF. Using three-phase flow of immiscible liquids to prevent coalescence of droplets in microfluidic channels: criteria to identify the third liquid and validation with protein crystallization. *Langmuir*. 2007;23:2255–2260.
27. Christopher GF, Noharuddin NN, Taylor JA, Anna SL. Experimental observations of the squeezing-to-dripping transition in T-shaped microfluidic junctions. *Phys Rev E*. 2008;78:036317.
28. Shui L, van den Berg A, Eijkel JCT. Capillary instability, squeezing, and shearing in head-on microfluidic devices. *J Appl Phys*. 2009;106:124305.
29. Xu JH, Li SW, Tan J, Luo GS. Correlations of droplet formation in T-junction microfluidic devices: from squeezing to dripping. *Microfluid Nanofluid*. 2008;5:711–717.
30. Cubaud T, Mason TG. Capillary threads and viscous droplets in square microchannels. *Phys Fluids*. 2008;20:053302.
31. Humphry KJ, Ajdari A, Fernandez-Nieves A, Stone HA, Weitz DA. Suppression of instabilities in multiphase flow by geometric confinement. *Phys Rev E*. 2009;79:056310.
32. Glawdel T, Elbuken C, Ren CL. Droplet formation in microfluidic T-junction generators operating in the transitional regime. II. Modeling. *Phys Rev E*. 2012;85:016323.
33. Wang K, Lu YC, Qin K, Luo GS, Wang T. Generating gas-liquid-liquid three-phase microflows in a cross-junction microchannel device. *Chem Eng Technol*. 2013;36:1047–1060.
34. Oskooei S, Sinton D. Partial wetting gas-liquid segmented flow microreactor. *Lab Chip*. 2010;10:1732–1734.
35. Pohar A, Lakner M, Plazl I. Parallel flow of immiscible liquids in a microreactor: modeling and experimental study. *Microfluid Nanofluid*. 2012;12:307–316.
36. Adamson DN, Mustafi D, Zhang J, Zheng B, Ismagilov RF. Production of arrays of chemically distinct nanolitre plugs via repeated splitting in microfluidic devices. *Lab Chip*. 2006;6:1178–1186.
37. Link DR, Anna SL, Weitz DA, Stone HA. Geometrically mediated breakup of drops in microfluidic devices. *Phys Rev Lett*. 2004;92:054503.
38. Wang K, Lu YC, Xu JH, Tan J, Luo GS. Generation of micromonodispersed droplets and bubbles in the capillary embedded T-junction microfluidic devices. *AIChE J*. 2011;57:299–306.
39. Utada AS, Fernandez-Nieves A, Stone HA, Weitz DA. Dripping to jetting transitions in coflowing liquid streams. *Phys Rev Lett*. 2007;99:94502.
40. Nie ZH, Seo MS, Xu SQ, Lewis PC, Mok M, Kumacheva E, Whitesides GM, Garstecki P, Stone HA. Emulsification in a microfluidic flow-focusing device: effect of the viscosities of the liquids. *Microfluid Nanofluid*. 2008;5:585–594.

Appendix

The rectification of gas flow rate is based on the average bubble length in the main channel. In an assistant experiment, only gas/liquid microflows were produced in a T-junction microchannel having the same cross-section as the double T-junction microchannel. As shown in Figure A1, the assistant microchannel was contacted to a wide monitor chamber (cross-section: 2 mm × 0.6 mm), where the gas slugs changed to gas disks. The average disk diameter d_{G1} was then measured and the slug volume was calculated by Eq. A1, provided by Nie et al.[40]

$$V_{G1} = \frac{\pi}{12}\left[2{d_{G1}}^3 - (d_{G1} - H)^2(2d_{G1} + H)\right] \qquad \text{(A1)}$$

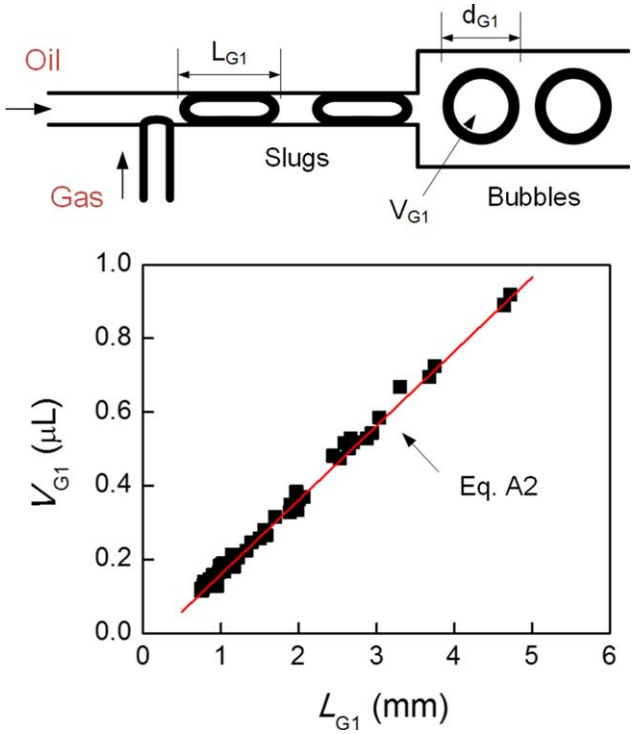

Figure A1. Scheme diagram of the assistant gas/liquid microflow experiment and the relation between average bubble length and average volume.

[Color figure can be viewed in the online issue, which is available at wileyonlinelibrary.com.]

where H is the height of the monitor channel. The relation between the average slug length and the average bubble volume was then established as shown by Eq. A2 and Figure A1

$$V_{G1}=0.2017(\text{mm}^2)L_{G1}-0.0424(\mu\text{L}) \quad \text{(A2)}$$

In the three-phase experiment, using the measured average bubble lengths in the double T-junction microchannel, the average volumes of bubbles were calculated. A gas flow rate rectification was then proceeded using the average slug volumes and the bubble generation frequencies, recorded by the experimental videos

$$Q_G=V_{G1}\cdot f_{G1} \quad \text{(A3)}$$

All the gas flow rates used to data analysis and model establishment were rectified flow rates in this article.

Manuscript received Sep. 20, 2014, and revision received Dec. 28, 2014.